Journal Pre-proofs

Synthesis of a Gemcitabine-Modified Phospholipid and its Subsequent Incorporation into a Single Microbubble Formulation Loaded with Paclitaxel for the Treatment of Pancreatic Cancer using Ultrasound-Targeted Microbubble Destruction

Keiran A. Logan, Heather Nesbitt, Bridgeen Callan, Jinhui Gao, McKaig T, Mark Taylor, Mark Love, Anthony P. McHale, John F. Callan

PII: S0939-6411(21)00148-X
DOI: https://doi.org/10.1016/j.ejpb.2021.05.018
Reference: EJPB 13589

To appear in: *European Journal of Pharmaceutics and Biopharmaceutics*

Received Date: 8 February 2021
Revised Date: 5 May 2021
Accepted Date: 18 May 2021

Please cite this article as: K.A. Logan, H. Nesbitt, B. Callan, J. Gao, M. T, M. Taylor, M. Love, A.P. McHale, J.F. Callan, Synthesis of a Gemcitabine-Modified Phospholipid and its Subsequent Incorporation into a Single Microbubble Formulation Loaded with Paclitaxel for the Treatment of Pancreatic Cancer using Ultrasound-Targeted Microbubble Destruction, *European Journal of Pharmaceutics and Biopharmaceutics* (2021), doi: https://doi.org/10.1016/j.ejpb.2021.05.018

Synthesis of a Gemcitabine-Modified Phospholipid and its Subsequent Incorporation into a Single Microbubble Formulation Loaded with Paclitaxel for the Treatment of Pancreatic Cancer using Ultrasound-Targeted Microbubble Destruction.

Keiran A. Logan[1], Heather Nesbitt[1], Bridgeen Callan[1], Jinhui Gao[1], McKaig T[1], Mark Taylor[2], Mark Love[3], Anthony P. McHale[1], John F. Callan[1*]

1. Biomedical Sciences Research Institute, University of Ulster, Coleraine, Northern Ireland, UK; 2. Department of HPB Surgery, Mater Hospital, Belfast, Northern Ireland, U.K. BT14 6AB. 3. Imaging Centre, The Royal Victoria Hospital, Grosvenor Road, Belfast, Northern Ireland, U.K. BT12 6BA

* Address to whom correspondence should be addressed: j.callan@ulster.ac.uk.

Abstract: Gemcitabine and nab-paclitaxel (Abraxane®) is a standard of care chemotherapy combination used in the treatment of patients with advanced pancreatic cancer. While the combination has shown a survival benefit when compared to gemcitabine monotherapy, it is associated with significant off-target toxicity. Ultrasound targeted microbubble destruction (UTMD) has emerged as an effective strategy for the site-specific deposition of drug-payloads. However, loading a single microbubble formulation with two drug payloads can be challenging and often involves several manipulations post-microbubble preparation that can be cumbersome and generally results in low / inconsistent drug loadings. In this manuscript, we report the one-pot synthesis of a gemcitabine functionalised phospholipid and use it to successfully generate stable microbubble formulations loaded with gemcitabine (Lipid-Gem MB) or a combination of gemcitabine and paclitaxel (Lipid-Gem-PTX MB). Efficacy of the Lipid-Gem MB and Lipid-Gem-PTX MB formulations, following ultrasound (US) stimulation, was evaluated in a three-dimensional (3D) PANC-1 spheroid model of pancreatic cancer and a mouse model bearing ectopic BxPC-3 tumours. The results demonstrated a significant reduction in the cell viability in spheroids for both formulations reducing from 90 ± 10% to 62 ± 5% for Lipid-Gem MB and 84 ± 10% to 30 ± 6% Lipid-Gem-PTX MB following US irradiation.

When compared with a clinically relevant dose of free gemcitabine and paclitaxel (i.e. non-particle bound) in a BxPC-3 murine pancreatic tumour model, both formulations also improved tumour growth delay with tumours 40 ± 20% and 40 ± 30% smaller than the respective free drug formulation when treated with Lipid-Gem MB and Lipid-Gem-PTX MB respectively, at the conclusion of the experiment. These results highlight the potential of UTMD mediated Gem / PTX as a treatment for pancreatic cancer and the facile preparation of Lipid-Gem-PTX MBs using a gemcitabine functionalised lipid should expedite clinical translation of this technology.

Keywords: Microbubble, ultrasound, transphosphatidylation, pancreatic cancer, gemcitabine, paclitaxel.

Introduction: Pancreatic cancer has the lowest survival rate among the 21 most common forms of cancer with 458,918 new cases and 432,242 deaths reported worldwide in 2018 alone. [1] Pancreatic ductal adenocarcinoma (PDAC) accounts for the vast majority (75-85 %) of all pancreatic neoplasms. [2,3] Surgery remains the only chance of a cure for PDAC and the survival rate for patients who receive surgery is significantly improved. [4] However, only 15-20 % of patients are eligible for surgery at the point of diagnosis with the remaining patients presenting with locally advanced or metastatic disease. [5]

Gemcitabine (Gem), in combination with nanoparticle bound paclitaxel (nPTX), improves survival in patients with advanced pancreatic cancer when compared to gemcitabine monotherapy and is commonly used in the neo-adjuvant and adjuvant settings. [6,7] However, the modest 1.8-month improvement in median overall survival observed for Gem-nPTX v Gem monotherapy comes at a cost of increased off-target side-effects with the incidence of leukopenia and febrile neutropenia significantly enhanced. Therefore, Gem-nPTX is typically only recommended for patients with Karnofsky performance status (KPS) of greater than 70%. [8] Therefore, there is a need to develop innovative solutions to enable a more targeted delivery of this drug combination to maximise efficacy while reducing off-target toxicity, thereby broadening its use in a greater number of patients.

Ultrasound targeted microbubble destruction (UTMD) has emerged as a novel approach to targeted drug delivery enabling the administration of significantly reduced amounts of chemotherapy while maintaining, or in some cases enhancing, the therapeutic effect. [9] Microbubbles (MBs) are gas filled microspheres stabilised with a coating material often composed of lipid, protein or polymers. [10] When exposed to ultrasound (US), the high compressibility of MBs allow them to expand and contract in the low- and high- pressure regions of the US wave. At certain acoustic amplitudes (50-200 kPa), MBs oscillate non-linearly resulting in US signals which can significantly improve the quality of diagnostic US imaging. [11] At higher amplitudes, MBs can undergo rapid expansion followed by violent collapse, destroying the MBs and releasing their contents into the surrounding tissue. Furthermore, as a result of this violent collapse, extremely high localised temperatures and pressures are generated which are often accompanied by shockwaves and high-speed fluid microjets which can, in turn, induce transient pitting in cell membranes facilitating the uptake of certain drugs into cells. [12] This site-specific MB destruction has enabled the delivery of various clinically useful payloads including chemotherapy and nucleic acids as well as gaseous payloads including oxygen, nitric oxide and noble gases, by either loading into / onto the MB shell or within its core. [13–17] Given the clinical benefit associated with Gem/nPTX treatment for pancreatic cancer, we were keen to develop a MB formulation containing both Gem and PTX and assess the resulting formulation for UTMD mediated efficacy in an *in vitro* three-dimensional (3D) model of human primary pancreatic carcinoma (PANC-1) cell line and murine BxPC-3 model of pancreatic cancer.

Our previous work has demonstrated the effectiveness of UTMD in targeting the delivery of drug payloads to solid tumours. [9,15] The hydrophobic acyl layer of the MB shell was used to load hydrophobic drugs [9] while hydrophilic drugs were attached to the surface using a biotin-avidin interaction. [15] The latter involved functionalising the hydrophilic drug with biotin and then attaching it to the MB surface which was pre-loaded with avidin. However, while this approach is effective in proof-of-principle studies, it has two main shortcomings. First, it is cumbersome from a manufacturing perspective requiring several manipulations post

MB formation to attach the drug payload. Second, avidin is a high molecular weight protein while biotin is a small molecule and this mismatch in molecular weight means the maximum theoretical wt/wt loading of a biotinylated payload to avidin is low. Therefore, we were keen to develop a single MB formulation, loaded with Gem and PTX, that did not require the biotin-avidin cross link or any other manipulation post MB formation to attach the drug payloads.

To enable this, a gemcitabine functionalised phospholipid (Lipid-Gem) was synthesised and used as the main lipid constituent of MBs that also contained PTX hydrophobically embedded within the acyl layer of the MB shell. To the best of our knowledge, this is the first time a lipid-drug conjugate such as lipid-Gem has been used to prepare drug-loaded MBs in a single step. The resulting formulation was assessed for UTMD mediated efficacy in a 3D spheroid PANC-1 model and murine BxPC-3 model of pancreatic cancer.

2.0 Materials and methods

2.1. Materials, reagents and equipment: Reagents and solvents were purchased from commercial sources at the highest possible grade. PANC-1 and BxPC-3 cells were obtained from the American Type Culture Collection (ATCC) (Manassas, VA, USA) and Matrigel from BD Biosciences (San Jose, CA, USA). SCID mice (C.B-17/IcrHanHsd-PrkdcSCID) were bred in house. 1,2-dibehenoyl-sn-glycero-3-phosphocholine (DBPC) and 1,2-distearoyl-sn-glycero-3-phosphoethanolamine-N-[methoxy(polyethylene glycol)-2000] (ammonium salt) (DSPE-PEG (2000)) were purchased from Avanti Polar Lipids (Alabaster, AL, USA). Paclitaxel and gemcitabine hydrochloride were purchased from XABC (Shaanxi, China). Phospholipase D from *Streptomyces* sp (enzyme activity >200 U/mg) was purchased from Sekisui Diagnostics (Maidstone, UK). MBs were formed using a Microson ultrasonic cell disruptor, 100 W, 22.5 kHz, from Misonix Inc. (Farmingdale, NY, USA). Optical microscope images of microbubbles were obtained using an optical compound microscope (Amscope, Irvine, CA, USA) while optical images of spheroids were obtained using a ZEISS Primovert inverted microscope (ZEISS, Oberkochen, Germany). UV-Vis spectra were recorded with a Varian Cary spectrophotometer (Palo Alto, CA, USA), using quartz cells (path length = 1 cm). UV

absorbance of MTT was analysed using a Fluostar Omega plate reader (BMG Labtech, Ortenberg, Germany). NMR spectra were obtained on Varian 500 MHz instrument at 25.0 ± 1 °C (Palo Alto, CA, USA) and processed using TopSpin software (Bruker, Billerica, MA, USA). MALDI-TOF mass spectra were obtained using an AB SCIEX 4800 MALDI-TOF system (Framingham, MA, USA) with an α-Cyano-4-hydroxycinnamic acid matrix. RP-HPLC analysis was carried out on a Shimadzu Prominence system (Shimadzu Corp., Kyoto, Japan). Ultrasound treatments were performed using a Sonidel SP100 Sonoporator fitted with a 1 MHz transducer (diameter = 1.38 cm, effective radiating area = 0.8 cm^2) (Sonidel Limited, Dublin, Ireland).

*2.2. Synthesis of (2R)-3-(((((2R,3R,5R)-5-(4-amino-2-oxopyrimidin-1(2H)-yl)-4,4-difluoro-3-hydroxytetrahydrofuran-2-yl)methoxy)(hydroxy)phosphoryl)oxy)propane-1,2-diyl didocosanoate (Lipid-Gem)***:** A chloroform solution (20 mL) containing DBPC (500 mg, 480 µmol) was added to a stirred solution of gemcitabine hydrochloride (400 mg, 1.5 mmol) and phospholipase D from *Streptomyces* sp (3 mg, 900 units) in sodium acetate buffer (200 mM, pH 4.5, 5 mL) containing calcium chloride (200 mM). The mixture was stirred vigorously at 45°C for 6 hours after which a solution containing chloroform (10 mL) and methanol (15 mL) was added. The organic layer was separated, and the aqueous layer washed twice with a chloroform/methanol mixture (2:1 v/v). The organic extracts were combined, dried using anhydrous sodium sulphate, filtered and concentrated *in vacuo*. The crude product was purified using preparative thin layer chromatography (chloroform:methanol:(7N) ammonium hydroxide (65:25:4 v/v)) to give Lipid-Gem as a white solid (127 mg, 25% yield). ^{1}H NMR (500 MHz, $CDCl_3$:CD_3OD (2:1)) δ (ppm) 7.83 (*d*, 1H, CH), 6.40 (*s,* 1H, CH) 5.91 (*d*, 1H, CH), 5.40 (*m*, 1H, glycerol CH), 3.90-4.40 (*m*, 9H, 3'(CH), 2'(CH) 4'(CH), 5'(CH_2) glycerol CH_2, glycerol CH_2OPO), 2.27 (*m*, 4H, 2x $COCH_2$), 1.57 (*m*, 4H, 2xCH_2), 1.23 (*m*, 72H, behenoyl CH_2), 0.83 (*t*, 6H, 2xCH_3). Positive mode MALDI-TOF $[M+H]^+$: calculated for $C_{56}H_{102}F_2N_3O_{11}P$ = 1061.7220 Da, found = 1062.7800 Da.

2.3. *Preparation of Lipid-Gem microbubbles (Lipid-Gem MB) and Lipid-Gem MB loaded with PTX (Lipid-Gem-PTX MB):* For the preparation of Lipid-Gem MB**,** Lipid-Gem (5 mg, 4.71 µmol) and DSPE-PEG (2000) (1.43 mg, 0.51 µmol) were dissolved in a mixture of chloroform and methanol (2:1 v/v, 100 µL) and then placed in a vacuum oven at 40^{o}C for 1 hour to allow the solvent to evaporate. The dried lipid film was rehydrated in a mixture of PBS, glycerol and propylene glycol (8:1:1) (PGP) and stirred at 90^{o}C for 1 hour. The lipid suspension was then sonicated using a probe sonicator at amplitude setting 25% for 1 min to form multilamellar vesicles. The headspace of the vial was then filled using a stream of perfluorobutane (PFB) gas and the tip of the probe was positioned at the gas-liquid interface. The lipid suspension was further sonicated at amplitude setting 90% for 30 seconds to form a milky white MB suspension. This suspension was centrifuged (5 min, 100 RCF) and the infranatant was removed and replaced with fresh PGP (2 mL). This centrifugation process was repeated a further time and the resultant MB cake was re-suspended in PGP (2 mL). For the preparation of Lipid-Gem-PTX MB, the above procedure was also followed but PTX (2.5 mg, 2.93 µmol) was incorporated with the Lipid-Gem and DSPE-PEG (2000) in the first step. Both MB formulation were stored on ice and used within 3 hours.

2.4. Characterisation of MB size and concentration: An aliquot of freshly prepared MB suspension was diluted in cold PGP. A 10 µL sample was then loaded onto a haemocytometer and MB were allowed to rise to surface of the cover slide for 5 mins before microscope images (x40 objective) (n=20) were collected and saved as high-resolution TIFF files. These images were then analysed using a bespoke MATLAB algorithm as described in [18]. Based on the known area per pixel and known frame volume, the distribution of MB diameters and mean MB concentration was determined.

2.5. Determination of PTX loading in Lipid-Gem-PTX MB: A sample of MBs were destroyed using an ultrasonic bath and a volume of the resulting solution was diluted in a mixture of acetonitrile and water (1:1 v/v). This sample was then analysed using RP-HPLC. A volume of

50 μL was injected onto a Phenomenex C_{18} column (250 × 4.6 mm, 5 μm) and the sample was eluted using a mobile phase consisting of acetonitrile and water (1:1 v/v), a flow rate of 1.5 mL/min and a detection wavelength of 227 nm. The loading of PTX was determined with reference to a standard calibration curve (R^2 = 0.9997) and expressed as μg/10^8 MBs.

2.6. Determination of Gem loading in Lipid-Gem-MB and Lipid-Gem-PTX MB: A sample of MBs were destroyed using an ultrasonic bath and a volume of the resulting solution was diluted in a mixture of chloroform and methanol (1:20 v/v). This sample was then analysed using UV-Vis spectrophotometry. A volume of 700 μL was loaded into a quartz cuvette and the absorbance of the sample was read at 267 nm. The loading of Lipid-Gem was determined with reference to a standard calibration curve (R^2 = 0.9974) and expressed as μg/10^8 MBs.

2.7. Formation of PANC-1 spheroids: The human primary pancreatic carcinoma cell line PANC-1 was maintained in Dulbecco's Modified Eagle's Medium (DMEM) containing 1 g/L glucose and supplemented with penicillin (100 U/mL), streptomycin (100 mg/mL), and fetal bovine serum (10% v/v). Cells were incubated at 37°C in a humidified atmosphere with 5% CO_2. An agarose solution in DMEM (1.5% w/v, 60 μL) was added to the wells of flat-bottomed 96-well plates and allowed to dry overnight before a suspension of PANC-1 cells were seeded at a density of 2000 cells per well in 200 μL of DMEM. Cells were incubated for a further 4 days to initiate spheroid formation and the medium (200 μL) was replaced every other day.

2.8. UTMD mediated cytotoxicity of Lipid-Gem MB and Lipid-Gem-PTX MB in PANC-1 Spheroids: PANC-1 spheroids were prepared as described above. The medium in each well was replaced with either fresh medium, a suspension of Lipid-Gem-PTX MB ([Lipid-Gem] = 10 μM, [PTX] = 6.2 μM, 3 x10^7 MB). Wells were then treated immediately with US (1 MHz, 3.5 W/cm^2 (SATP), DC = 30%, PRF = 100 Hz, PNP = 0.48 MPa, time = 30 seconds) from below each well. Two days after initial treatment, cell viability was determined using an MTT assay.

A total of 4 spheroids per replicate from each condition were collected in an Eppendorf tube, washed with PBS and then incubated with trypsin/EDTA for 15 min at 37°C. The resultant cellular suspension was centrifuged (100 RCF, 5 min) and resuspended in a solution of MTT (100 µL, 5 mg/mL in DMEM) which was incubated for 3 hours. The cell suspension was then centrifuged (100 RCF, 5 min) and the pellet was dissolved in 100 µL of DMSO. The solution was transferred to a 96-well plate and the absorbance was measured at 570 nm using FLUOstar Omega microplate reader. Data were expressed as cell viability (%) compared to untreated controls.

2.9. UTMD mediated cytotoxicity of Lipid-Gem MB and Lipid-Gem-PTX MB in SCID mice bearing BxPC-3 ectopic tumours: All animals were treated humanely and in accordance with licensed protocols under the Animals (Scientific Procedures) Act 1986 Amendment Regulations 2012 (ASPA 2012). The human primary pancreatic carcinoma cell line, BxPC-3, was maintained in RPMI 1640 supplemented with penicillin (100 U/mL), streptomycin (100 mg/mL), and fetal bovine serum (10%) in a humidified 5% CO_2 atmosphere at 37°C. BxPC-3 cells (5 x10^6) in 100 µL of a mixture of Matrigel and RPMI (1:1 v/v) were sub-cutaneously implanted into the rear dorsum of 8-week old SCID mice (C.B-17/IcrHan®Hsd-Prkdcscid) (25 animals, 8 females and 17 males, starting weight = 25 ± 3 g). Palpable tumours appeared approximately 1-2 weeks after cell implantation. Once tumours became palpable, dimensions were measured using Vernier callipers. Tumour volume was calculated using the equation: tumour volume = (length × width^2)/2. [19] Animals were randomly separated into 4 treatment groups with the 5th group being an untreated control (mean volume 150 ± 140 mm^3). Group 1 received an intravenous (IV) bolus injection (100 µL) of Lipid-Gem MB (1 x$10^9 \pm 2$ x10^7 MB/mL, [Lipid-Gem] = 2.8 $\pm$ 0.3 mg/kg Gem); Group 2 received an IV injection (100 µL) of Lipid-Gem-PTX MB (8.6 x$10^8 \pm 1$ x10^7 MB/ mL, [Lipid-Gem] = 3.2 $\pm$ 0.4 mg/kg, [PTX] = 2.0 $\pm$ 0.2 mg/kg); Group 3 received an intraperitoneal (IP) injection (100 µL) of Gem HCl in PBS (120 mg/kg); Group 4 received an IP injection (100 µL) of Gem HCl in sterile PBS (120 mg/kg) in addition

to an IV injection (100 µL) of PTX in PBS:ethanol:Cremophor EL (8:1:1 v/v) (15 mg/kg). For groups 3 and 4, the dose, dosing frequency and route of administration were informed by previous reports in preclinical murine models of cancer. [20,21] For groups 2 and 3, US was applied directly to the tumour site using a Sonidel SP100 sonoporator (3.5 W/cm^2 (SATP), 1 MHz, DC = 30%, and PRF = 100 Hz, PNP = 0.48 MPa, 3.5 min) during injection and for a total duration of 3.5 min. Animals were treated on days 0, 4 and 6, and tumour volume and subject weight were recorded periodically for a total of 8 days.

2.10. Statistical analysis: Statistical analysis was carried out using Prism v8.4.0 software (Graphpad, SanDiego, CA, USA). *In vitro* and *in vivo* data are expressed as ± Standard Error of the Mean (SEM). A Student's t-test was used for direct comparisons of mean values. A P value of less than 0.05 was considered statistically significant.

3.0. Results and discussion: Lipid-Gem was synthesised using a transphosphatidylation reaction between DBPC and Gem catalysed by phospholipase D from *Streptomyces* sp (Scheme 1). Catalysis involves the hydrolysis of DBPC and selective esterification of the resulting phosphatidyl unit with the 5'-hydroxyl group of Gem. Following completion of the reaction, the crude product was purified using preparative-TLC providing Lipid-Gem as a white solid at a yield of 25%. While this yield may appear modest, the alternative approach to Lipid-Gem using a conventional linear synthesis is complex, involving several protection / deprotection steps to prevent the alternative condensation reactions possible at both the 3'-hydroxyl and cytidine amine groups of Gem.

Confirmation of Lipid-Gem formation was first assessed qualitatively by analytical TLC (Figure 1). Following elution, the TLC plate pre-spotted with both Lipid-Gem and Gem was visualised using UV (254 nm) and also stained with Dittmer-Lester reagent which is a selective stain for phosphate groups. This analysis suggested a successful reaction occurred between DPBC and Gem as the single UV active spot (R_f = 0.4) observed for Gem stained negative for

the presence of a phosphate group, while the higher R_f spot (R_f = 0.6) associated with Lipid-Gem was both UV active and stained positive for the presence of a phosphate group. This analysis indicates that Lipid-Gem contains both a chromophore, consistent with Gem and a phosphate group, consistent with the phosphatidyl unit of DBPC.

Structural analysis of Lipid-Gem was confirmed by ^{1}H NMR and MALDI-TOF mass spectroscopy. The main structural changes expected following a successful transphosphatidylation reaction between DBPC and Gem is loss of the choline unit from DBPC and formation of a phosphodiester bond between the resulting phosphatidyl unit and 5'-hydroxyl group of Gem. [22–24] These changes are clearly illustrated in the stacked ^{1}H NMR spectra shown in Figure 3 with resonances corresponding to the choline methyl groups (3.15 ppm) and methylene protons (3.60 and 4.15 ppm), present in the spectrum of DBPC, being absent in the spectrum of Lipid-Gem. Similarly, the resonance corresponding to the methylene protons adjacent to the 5'-hydroxyl group observed at 3.75 ppm in Gem, shifted downfield to 4.15 ppm in Lipid-Gem, reflecting their new chemical environment adjacent to the phosphodiester group. Full assignment of the ^{1}H NMR spectrum of Lipid-Gem is provided in Figure S1 (supplementary materials) but the analysis provided above, in combination with the positive identification of Lipid-Gem in the MALDI-TOF mass spectrum (Figure 3), confirmed its successful formation.

Following the successful preparation of Lipid-Gem, the next step was to determine its ability to form US responsive MBs. (Scheme 2) Lipid-Gem MB were prepared using a standard thin-film hydration approach to form multilamellar vesicles (MLVs) consisting of Lipid-Gem along with the emulsifier DSPE-PEG (2000), followed by sonication in the presence of PFB gas to generate MBs. The resulting Lipid-Gem MB, were characterised in terms of mean particle diameter, mean particle concentration and drug loading. A representative microscope image of the suspension along with the corresponding size distribution is shown in Figure 4 and reveals spherical particles with a mean diameter of 2 ± 2 μm and a mean concentration of 2 x10^9 ± 2 x10^8 MB/mL, which are comparable with MBs prepared using the commercially sourced phospholipids described in previous publications. [9,15,19] The mean of loading of

Lipid-Gem was determined by UV-Vis analysis as 68 ± 7 μg/10^8 MBs representing an approximate loading of 25% Lipid-Gem in final MB formulation.

The Lipid-Gem-PTX MB formulation was prepared in a similar manner with the exception that PTX was also added to Lipid-Gem and DSPE-PEG (2000) prior to thin-film hydration. PTX it extremely hydrophobic with a LogP value of approximately 4 [20] resulting in an aqueous solubility of less than 0.01 mg/mL, and readily incorporates within the hydrophobic acyl layer of the MB shell during the self-assembly process. PTX incorporation did not negatively impact the size (2 ± 2 μm), MB number (1.7 x10^9 ± 0.1 x10^8 MB/mL) or Lipid-Gem loading (80 ± 10 μg/10^8 MBs) which all compared favourably to the Lipid-Gem MB (Figure 5). The PTX loading was determined using RP-HPLC as 49 ± 5 μg/10^8 MB and again compared favourably with previous reports of PTX loaded MBs. [9] Therefore, using Lipid-Gem enables an effective facile preparation of a single MB formulation carrying both PTX and Gem.

Having successfully prepared the Lipid-Gem MB and Lipid-Gem-PTX MB formulations, the next step was to determine their UTMD mediated efficacy in a three-dimensional (3D) spheroid model of PDAC. Where standard two-dimensional (2D) cell culture lacks the cell to cell and cell to extracellular matrix interactions required to bridge the gap between *in vitro* cell experimentation and *in vivo* animal models of cancer, 3D spheroids incorporate many important characteristics associated with the *in vivo* cellular environment, growth kinetics and response to anticancer agents. [27,28] PANC-1 spheroids were treated with Lipid-Gem MB or Lipid-Gem-PTX MB and exposed to US to induce inertial cavitation of the MBs. Untreated spheroids, spheroids treated with US only and spheroids treated with Lipid-Gem MB or Lipid-Gem-PTX MB in the absence of US were included as controls. Following treatment, cell viability was determined using an MTT assay. Optical images of the treated and untreated spheroids are shown in Figure 6 and reveal no visually apparent effects on spheroid morphology for those treated with US in the absence of MBs. Similarly, spheroids treated with Lipid-Gem MB in the absence of US also appeared visually intact. However, spheroids treated with Lipid-Gem MB and US appeared less cohesive in structure (i.e. has more shedding at

their edges) than those treated with Lipid-Gem MB alone (i.e. no US). This effect was amplified for spheroids treated with Lipid-Gem-PTX MB + US where a significant disruption in spheroid morphology was apparent with small areas of cellular debris evident around the perimeter of the spheroid corona. When spheroid viability was determined using an MTT assay (Figure 7), the proportion of viable cells remaining following treatment with Lipid-Gem MB + US or Lipid-Gem-PTX MB + US were significantly reduced relative to spheroids treated with US alone ($p = 0.033$ and $p = 0.0031$ respectively) or with the respective MB formulation alone (i.e. no US) ($p = 0.0336$ and $p = 0.0037$ respectively). Indeed, while the reduction in viability for spheroids treated with Lipid-Gem MB + US was 38 ± 5%, this reduced further to 70 ± 6% for Lipid-Gem-PTX MB + US ($p = 0.0077$), consistent with the visual effects apparent from the optical images shown in Figure 6.

To further investigate the efficacy of the MB formulation *in vivo*, BxPC-3 tumours were established in the rear dorsum of SCID mice and animals were treated with an IV injection of either Lipid-Gem MB or Lipid-Gem-PTX MB with US applied to the tumour during injection to induce MB destruction. The BxPC-3 model was chosen for the *in vivo* experiments as it develops hypoxic recalcitrant tumours and is routinely used in our laboratory enabling comparisons between different treatment approaches to be made. Separate groups of animals were also treated with a standard clinically relevant scaled dose (120 mg/kg) of free Gem (i.e. non-MB bound) or a combination of free Gem (120 mg/kg) and free PTX (15 mg/kg), administered in a Cremophor EL vehicle. The tumour growth delay curve is shown in Figure 8a and reveals modest tumour control for the free Gem group and free Gem + PTX group, with tumour volumes 45 ± 10% and 30 ± 10% larger than their starting volumes 8 days after the initial treatment, compared to 150 ± 30% growth for the untreated group. However, growth of tumours in animals treated with Lipid-Gem MB + US only increased by 7 ± 7%, while those treated with Lipid-Gem-PTX MB + US reduced by 10 ± 10% from their pre-treatment size, over the same time period. Interestingly, this significant improvement ($p = 0.0169$) in efficacy using the MB formulations was achieved using substantially lower doses of Gem (3.15 mg/kg) and PTX (1.98 mg/kg) representing 38.1 and 7.5-fold lower doses of Gem and PTX respectively.

As a result, both MB treatments were well tolerated with no significant reduction in body weight observed when compared to untreated animals (Figure 8b). In contrast, the weight of animals treated with free Gem / PTX reduced significantly by 14% ($p = 0.0008$) after 8 days highlighting the acute toxicity of this treatment. These results clearly demonstrate the effectiveness of UTMD using Lipid-Gem MB and Lipid-Gem-PTX MB in treating this model of pancreatic cancer. The precise mechanism of intracellular activation of Lipid-Gem remains uncertain. Previous studies have attributed the effectiveness of phospholipid-nucleoside prodrugs to two primary mechanisms. [23] First, their hydrophobic nature may enhance transport into the cell through passive diffusion thereby bypassing the need for nucleoside transporter proteins. Indeed, the downregulation of such proteins has been associated with resistance to Gem monotherapy. [24,25] Secondly, once inside the cell, metabolism by ubiquitous phospholipase D or C type enzymes could trigger the release of Gem or its active monophosphate derivative, with the latter circumventing the requirement for an initial kinase mediated phosphorylation step. [26,27]

In conclusion, a Gem modified phospholipid was successfully prepared in a one-pot reaction from the commercially available precursors DBPC and Gem. The Lipid-Gem was used to prepare Gem and Gem/PTX loaded MBs eliminating the need for biotin-avidin or other conjugation strategies to enable drug loading. UTMD mediated treatment of PANC-1 spheroids and BxPC-3 tumours in mice demonstrated that both formulations were efficacious and well tolerated. Given the need for more effective and well tolerated approaches for treating pancreatic cancer, coupled with the fact that all components of this treatment (i.e. MBs, US, Gem and PTX) are already approved for use in humans, UTMD using Lipid-Gem-PTX MB offers a promising alternative to existing treatments and clinical translation should be relatively straightforward.

Acknowledgements: KAL thanks the Department of the Economy in Northern Ireland for a PhD studentship. JFC thanks Norbrook Laboratories Ltd for an endowed chair.

Data availability. The raw/processed data required to reproduce these findings cannot be shared at this time due to technical limitations. However, any specific file(s) can be made available on request.

References:

(1) Bray, F.; Ferlay, J.; Soerjomataram, I.; Siegel, R. L.; Torre, L. A.; Jemal, A. Global Cancer Statistics 2018: GLOBOCAN Estimates of Incidence and Mortality Worldwide for 36 Cancers in 185 Countries. *CA. Cancer J. Clin.* **2018**, *68* (6), 394–424. https://doi.org/10.3322/caac.21492.

(2) Kleeff, J.; Korc, M.; Apte, M.; La Vecchia, C.; Johnson, C. D.; Biankin, A. V.; Neale, R. E.; Tempero, M.; Tuveson, D. A.; Hruban, R. H.; Neoptolemos, J. P. Pancreatic Cancer. *Nat. Rev. Dis. Prim.* **2016**, *2*. https://doi.org/10.1038/nrdp.2016.22.

(3) Orth, M.; Metzger, P.; Gerum, S.; Mayerle, J.; Schneider, G.; Belka, C.; Schnurr, M.; Lauber, K. Pancreatic Ductal Adenocarcinoma: Biological Hallmarks, Current Status, and Future Perspectives of Combined Modality Treatment Approaches. *Radiation Oncology*. BioMed Central Ltd. August 2019, pp 1–20. https://doi.org/10.1186/s13014-019-1345-6.

(4) Kamarajah, S. K.; Burns, W. R.; Frankel, T. L.; Cho, C. S.; Nathan, H. Validation of the American Joint Commission on Cancer (AJCC) 8th Edition Staging System for Patients with Pancreatic Adenocarcinoma: A Surveillance, Epidemiology and End Results (SEER) Analysis. *Ann. Surg. Oncol.* **2017**, *24* (7), 2023–2030. https://doi.org/10.1245/s10434-017-5810-x.

(5) Singhi, A. D.; Koay, E. J.; Chari, S. T.; Maitra, A. Early Detection of Pancreatic Cancer: Opportunities and Challenges. *Gastroenterology* **2019**, *156* (7), 2024–2040. https://doi.org/10.1053/j.gastro.2019.01.259.

(6) Von Hoff, D. D.; Ervin, T.; Arena, F. P.; Chiorean, E. G.; Infante, J.; Moore, M.; Seay, T.; Tjulandin, S. A.; Ma, W. W.; Saleh, M. N.; Harris, M.; Reni, M.; Dowden, S.; Laheru, D.; Bahary, N.; Ramanathan, R. K.; Tabernero, J.; Hidalgo, M.; Goldstein, D.; Van Cutsem, E.; Wei, X.; Iglesias, J.; Renschler, M. F. Increased Survival in Pancreatic Cancer with Nab-Paclitaxel plus Gemcitabine. *N. Engl. J. Med.* **2013**, *369* (18), 1691–1703. https://doi.org/10.1056/NEJMoa1304369.

(7) Miyasaka, Y.; Ohtsuka, T.; Kimura, R.; Matsuda, R.; Mori, Y.; Nakata, K.; Kakihara, D.; Fujimori, N.; Ohno, T.; Oda, Y.; Nakamura, M. Neoadjuvant Chemotherapy with Gemcitabine Plus Nab-Paclitaxel for Borderline Resectable Pancreatic Cancer Potentially Improves Survival and Facilitates Surgery. *Annals of Surgical Oncology*. Springer New York LLC March 2019, pp 1528–1534. https://doi.org/10.1245/s10434-019-07309-8.

(8) Macarulla, T.; Pazo-Cid, R.; Guillén-Ponce, C.; López, R.; Vera, R.; Reboredo, M.; Martin, A. M.; Rivera, F.; Beveridge, R. D.; La Casta, A.; Valadés, J. M.; Martínez-Galán, J.; Ales, I.; Sastre, J.; Perea, S.; Hidalgo, M. Phase I/II Trial to Evaluate the Efficacy and Safety of Nanoparticle Albumin-Bound Paclitaxel in Combination with Gemcitabine in Patients with Pancreatic Cancer and an ECOG Performance Status of 2. In *Journal of Clinical Oncology*; American Society of Clinical Oncology, 2019; Vol. 37, pp 230–238. https://doi.org/10.1200/JCO.18.00089.

(9) Logan, K.; Foglietta, F.; Nesbitt, H.; Sheng, Y.; McKaig, T.; Kamila, S.; Gao, J.; Nomikou, N.; Callan, B.; McHale, A. P.; Callan, J. F. Targeted Chemo-Sonodynamic Therapy Treatment of Breast Tumours Using Ultrasound Responsive Microbubbles Loaded with Paclitaxel, Doxorubicin and Rose Bengal. *Eur. J. Pharm. Biopharm.* **2019**, *139*, 224–231. https://doi.org/10.1016/j.ejpb.2019.04.003.

(10) Stride, E.; Segers, T.; Lajoinie, G.; Cherkaoui, S.; Bettinger, T.; Versluis, M.; Borden, M. Microbubble Agents: New Directions. *Ultrasound in Medicine and Biology*. Elsevier USA June 2020, pp 1326–1343. https://doi.org/10.1016/j.ultrasmedbio.2020.01.027.

(11) De Jong, N.; Bouakaz, A.; Frinking, P. Basic Acoustic Properties of Microbubbles.

Echocardiography. Futura Publishing Company Inc. 2002, pp 229–240. https://doi.org/10.1046/j.1540-8175.2002.00229.x.

(12) Fan, Z.; Kumon, R. E.; Deng, C. X. Mechanisms of Microbubble-Facilitated Sonoporation for Drug and Gene Delivery. *Therapeutic Delivery*. Future Science Ltd 2014, pp 467–486. https://doi.org/10.4155/tde.14.10.

(13) Chattaraj, R.; Hwang, M.; Zemerov, S. D.; Dmochowski, I. J.; Hammer, D. A.; Lee, D.; Sehgal, C. M. Ultrasound Responsive Noble Gas Microbubbles for Applications in Image-Guided Gas Delivery. *Adv. Healthc. Mater.* **2020**, 1901721. https://doi.org/10.1002/adhm.201901721.

(14) Grishenkov, D.; Gonon, A.; Weitzberg, E.; Lundberg, J. O.; Harmark, J.; Cerroni, B.; Paradossi, G.; Janerot-Sjoberg, B. Ultrasound Contrast Agent Loaded with Nitric Oxide as a Theranostic Microdevice. *Drug Des. Devel. Ther.* **2015**, *9*, 2409–2419. https://doi.org/10.2147/DDDT.S77790.

(15) Nesbitt, H.; Sheng, Y.; Kamila, S.; Logan, K.; Thomas, K.; Callan, B.; Taylor, M. A.; Love, M.; O'Rourke, D.; Kelly, P.; Beguin, E.; Stride, E.; McHale, A. P.; Callan, J. F. Gemcitabine Loaded Microbubbles for Targeted Chemo-Sonodynamic Therapy of Pancreatic Cancer. *J. Control. Release* **2018**, *279*, 8–16. https://doi.org/10.1016/j.jconrel.2018.04.018.

(16) Cai, X.; Jiang, Y.; Lin, M.; Zhang, J.; Guo, H.; Yang, F.; Leung, W.; Xu, C. Ultrasound-Responsive Materials for Drug/Gene Delivery. *Frontiers in Pharmacology*. Frontiers Media S.A. January 2020, p 1650. https://doi.org/10.3389/fphar.2019.01650.

(17) Reusser, T. D.; Song, K. H.; Ramirez, D.; Benninger, R. K.; Papadopoulou, V.; Borden, M. A. Phospholipid Oxygen Microbubbles for Image-Guided Therapy. *Nanotheranostics* **2020**, *4* (2), 83–90. https://doi.org/10.7150/ntno.43808.

(18) Sennoga, C. A.; Mahue, V.; Loughran, J.; Casey, J.; Seddon, J. M.; Tang, M.; Eckersley, R. J. On Sizing and Counting of Microbubbles Using Optical Microscopy. *Ultrasound Med. Biol.* **2010**, *36* (12), 2093–2096. https://doi.org/10.1016/j.ultrasmedbio.2010.09.004.

(19) Euhus, D. M.; Hudd, C.; Laregina, M. C.; Johnson, F. E. Tumor Measurement in the Nude Mouse. *J. Surg. Oncol.* **1986**, *31* (4), 229–234. https://doi.org/10.1002/jso.2930310402.

(20) Sugisawa, N.; Miyake, K.; Higuchi, T.; Oshiro, H.; Zhang, Z.; Park, J. H.; Kawaguchi, K.; Chawla, S. P.; Bouvet, M.; Singh, S. R. A. M.; Unno, M.; Hoffman, R. M. Induction of Metastasis by Low-Dose Gemcitabine in a Pancreatic Cancer Orthotopic Mouse Model: An Opposite Effect of Chemotherapy. *Anticancer Res.* **2019**, *39* (10), 5339–5344. https://doi.org/10.21873/anticanres.13726.

(21) Desai, N.; Trieu, V.; Yao, Z.; Louie, L.; Ci, S.; Yang, A.; Tao, C.; De, T.; Beals, B.; Dykes, D.; Noker, P.; Yao, R.; Labao, E.; Hawkins, M.; Soon-Shiong, P. Increased Antitumor Activity, Intratumor Paclitaxel Concentrations, and Endothelial Cell Transport of Cremophor-Free, Albumin-Bound Paclitaxel, ABI-007, Compared with Cremophor-Based Paclitaxel. *Clin. Cancer Res.* **2006**, *12* (4), 1317–1324. https://doi.org/10.1158/1078-0432.CCR-05-1634.

(22) Shuto, S.; Awano, H.; Shimazaki, N.; Hanaoka, K.; Matsuda, A. Nucleosides and Nucleotides. 150. Enzymatic Synthesis of 5′-Phosphatidyl Derivatives of 1-(2-C-Cyano-2-Deoxy-β-D-Arabino-Pentofuranosyl)Cytosine (CNDAC) and Their Notable Antitumor Effects in Mice. *Bioorganic Med. Chem. Lett.* **1996**, *6* (9), 1021–1024. https://doi.org/10.1016/0960-894X(96)00162-X.

(23) Shuto, S.; Itoh, H.; Sakai, A.; Nakagami, K.; Imamura, S.; Matsuda, A. Nucleosides and Nucleotides-CXXXVII. Antitumor Phospholipids with 5-Fluorouridine as a Cytotoxic Polar-Head: Synthesis of 5′-Phosphatidyl-5-Fluorouridines by Phospholipase d-Catalyzed Transphosphatidylation. *Bioorganic Med. Chem.* **1995**, *3* (3), 235–243. https://doi.org/10.1016/0968-0896(95)00003-Y.

(24) Shuto, S.; Ueda, S.; Imamura, S.; Fukukawa, K.; Matsuda, A.; Ueda, T. A Facile One-Step Synthesis of 5′-Phosphatidylnucleosides by an Enzymatic Two-Phase Reaction. *Tetrahedron Lett.* **1987**, *28* (2), 199–202. https://doi.org/10.1016/S0040-4039(00)95685-5.

(25) McEwan, C.; Kamila, S.; Owen, J.; Nesbitt, H.; Callan, B.; Borden, M.; Nomikou, N.; Hamoudi, R. A.; Taylor, M. A.; Stride, E.; McHale, A. P.; Callan, J. F. Combined Sonodynamic and Antimetabolite Therapy for the Improved Treatment of Pancreatic Cancer Using Oxygen Loaded Microbubbles as a Delivery Vehicle. *Biomaterials* **2016**, *80*, 20–32. https://doi.org/10.1016/j.biomaterials.2015.11.033.

(26) Surapaneni, M. S.; Das, S. K.; Das, N. G. Designing Paclitaxel Drug Delivery Systems Aimed at Improved Patient Outcomes: Current Status and Challenges. *ISRN Pharmacol.* **2012**, *2012*. https://doi.org/10.5402/2012/623139.

(27) Burdett, E.; Kasper, F. K.; Mikos, A. G.; Ludwig, J. A. Engineering Tumors: A Tissue Engineering Perspective in Cancer Biology. *Tissue Engineering - Part B: Reviews*. Tissue Eng Part B Rev June 1, 2010, pp 351–359. https://doi.org/10.1089/ten.teb.2009.0676.

(28) Wen, Z.; Liao, Q.; Hu, Y.; You, L.; Zhou, L.; Zhao, Y. A Spheroid-Based 3-D Culture Model for Pancreatic Cancer Drug Testing, Using the Acid Phosphatase Assay. *Brazilian J. Med. Biol. Res.* **2013**, *46* (7), 634–642. https://doi.org/10.1590/1414-431X20132647.

(29) Matsuda, A.; Ueda, T.; Obara, T.; Nakagami, K.; Yaso, M.; Yaginuma, S.; Tsujmo, M.; Saito, T. New Neplanocin Analogues II. Enzymatic One-Step Synthesis and Antitumor Activity of 6'-(3-Sn-Phosphatidyl)Neplanocin a Derivatives. *Nucleosides and Nucleotides* **1992**, *11* (2–4), 437–446. https://doi.org/10.1080/07328319208021716.

(30) Mackey, J. R.; Mani, R. S.; Selner, M.; Mowles, D.; Young, J. D.; Belt, J. A.; Crawford, C. R.; Cass, C. E. Functional Nucleoside Transporters Are Required for Gemcitabine Influx and Manifestation of Toxicity in Cancer Cell Lines. *Cancer Res.* **1998**, *58* (19).

(31) Gourdeau, H.; Clarke, M. L.; Ouellet, F.; Mowles, D.; Selner, M.; Richard, A.; Lee, N.; Mackey, J. R.; Young, J. D.; Jolivet, J.; Lafrenière, R. G.; Cass, C. E. Mechanisms of Uptake and Resistance to Troxacitabine, a Novel Deoxycytidine Nucleoside Analogue, in Human Leukemic and Solid Tumor Cell Lines. *Cancer Res.* **2001**, *61* (19).

(32) Haperen, V. W. T. R. van; Veerman, G.; Eriksson, S.; Boven, E.; Stegmann, A. P. A.; Hermsen, M.; Vermorken, J. B.; Pinedo, H. M.; Peters, G. J. Development and Molecular Characterization of a 2′,2′-Difluorodeoxycytidine-Resistant Variant of the Human Ovarian Carcinoma Cell Line A2780. *Cancer Res.* **1994**, *54* (15), 4138–4143.

(33) Kroep, J. R.; Loves, W. J. P.; van der Wilt, C. L.; Alvarez, E.; Talianidis, I.; Boven, E.; Braakhuis, B. J. M.; van Groeningen, C. J.; Pinedo, H. M.; Peters, G. J. Pretreatment Deoxycytidine Kinase Levels Predict in Vivo Gemcitabine Sensitivity. *Mol. Cancer Ther.* **2002**, *1* (6), 371–376.

Figures and diagrams

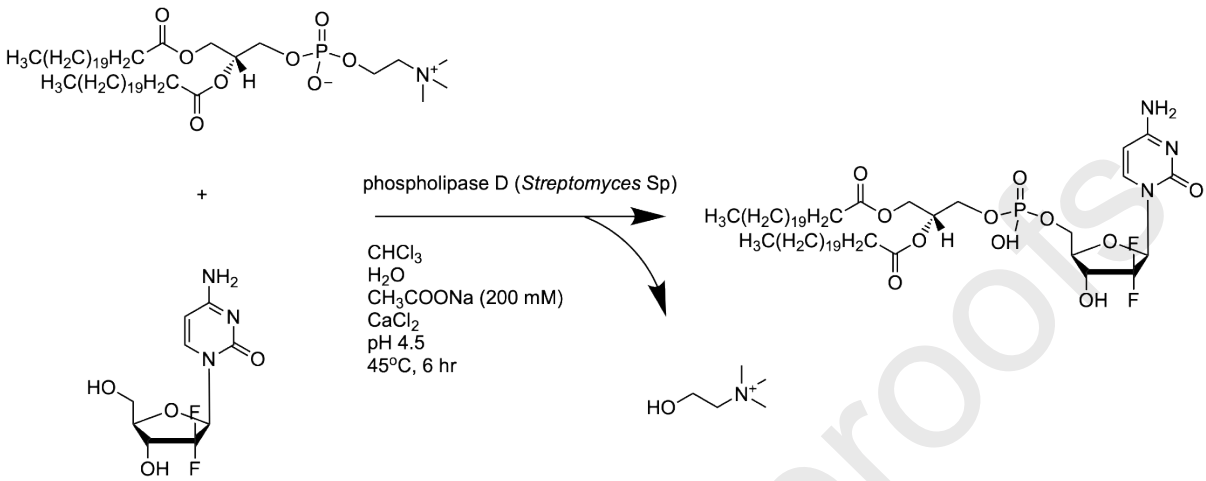

Scheme 1. Synthetic scheme for the preparation of Lipid-Gem.

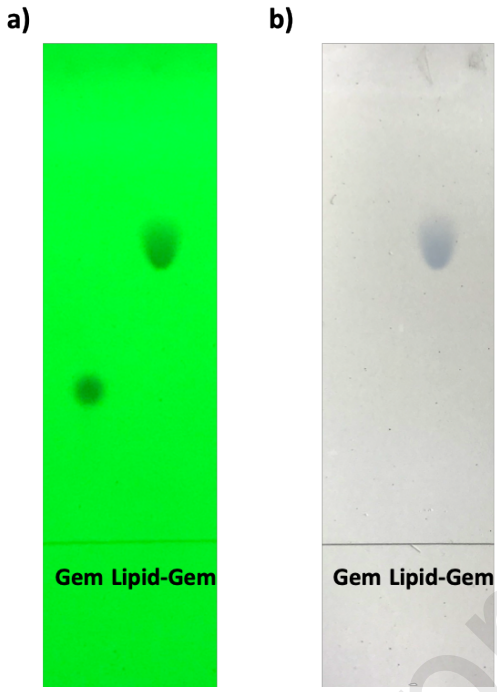

Figure 1. Images of TLC plates visualised under (a) UV irradiation and (b) following staining with Dittmer-Lester reagent (left spot – gemcitabine free base standard, right spot – purified Lipid-Gem).

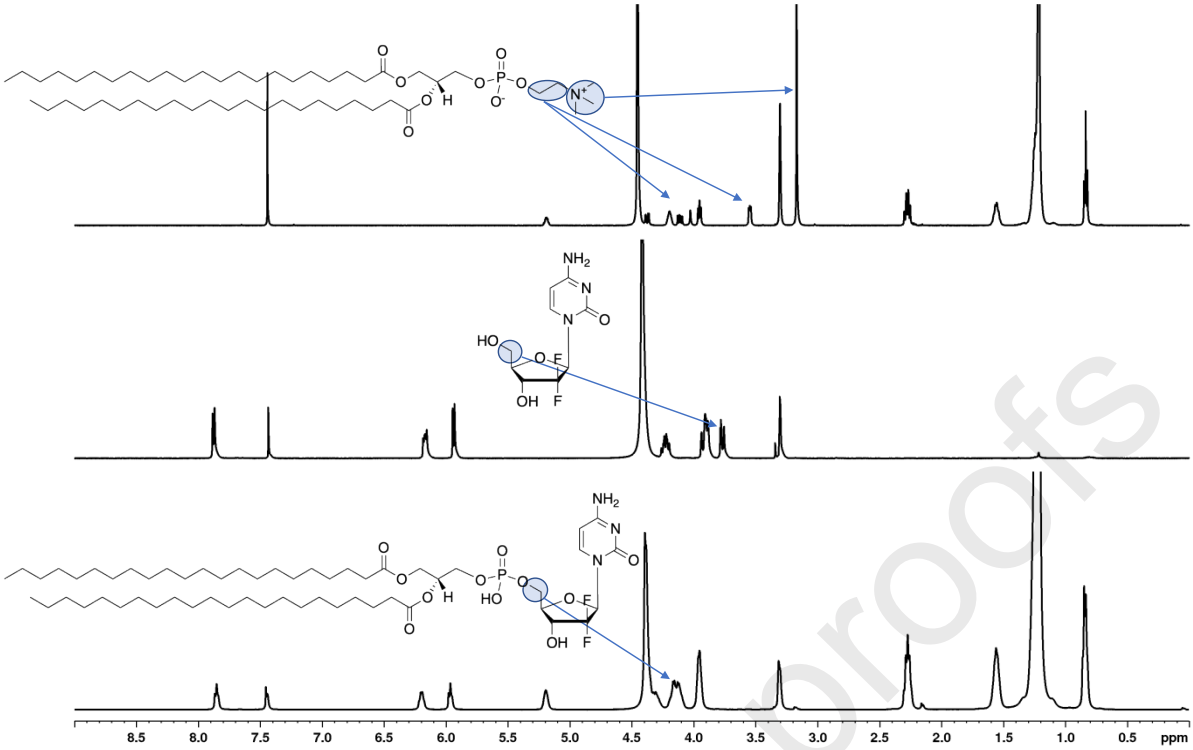

Figure 2. Stacked ^{1}H NMR spectra of DBPC standard (top), Gem (middle) and Lipid-Gem (bottom) recorded in $CDCl_3$:CD_3OD (2:1 v/v).

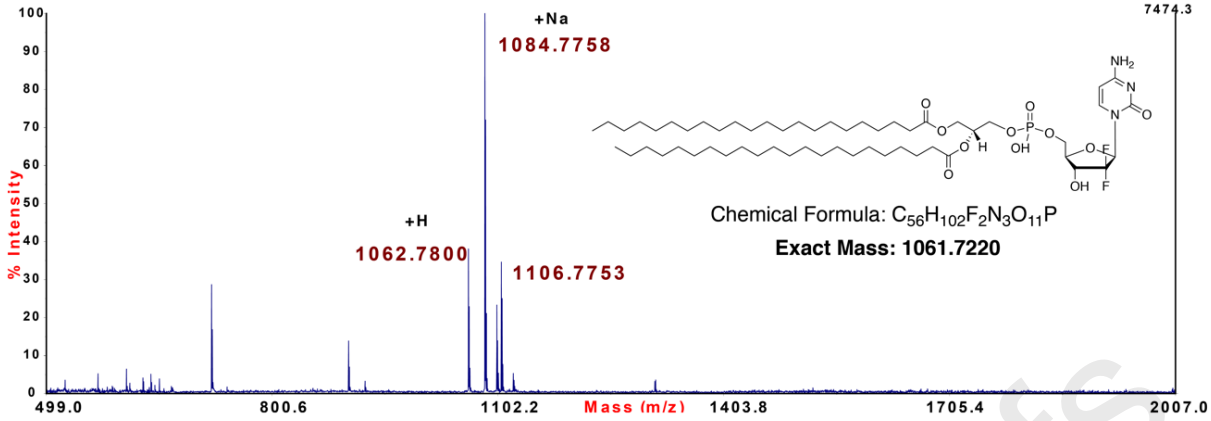

Figure 3. MALDI-TOF mass spectrum of Lipid-Gem recorded in $CHCl_3$:MeOH (2:1 v/v).

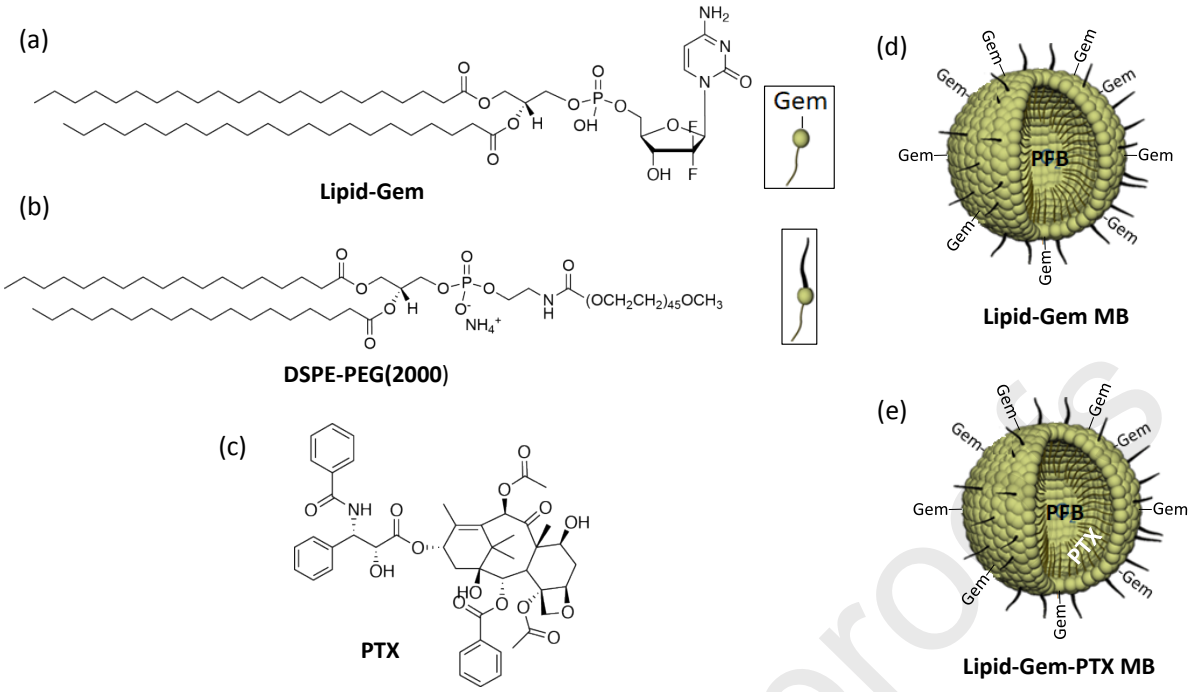

Scheme 2. Structures of (a) Lipid-Gem (b) DSPE-PEG (2000) and (c) PTX. (d) Schematic representation of Lipid-Gem MB and (e) schematic representation of Lipid-Gem-PTX MB. PFB refers to perfluorobutane gas.

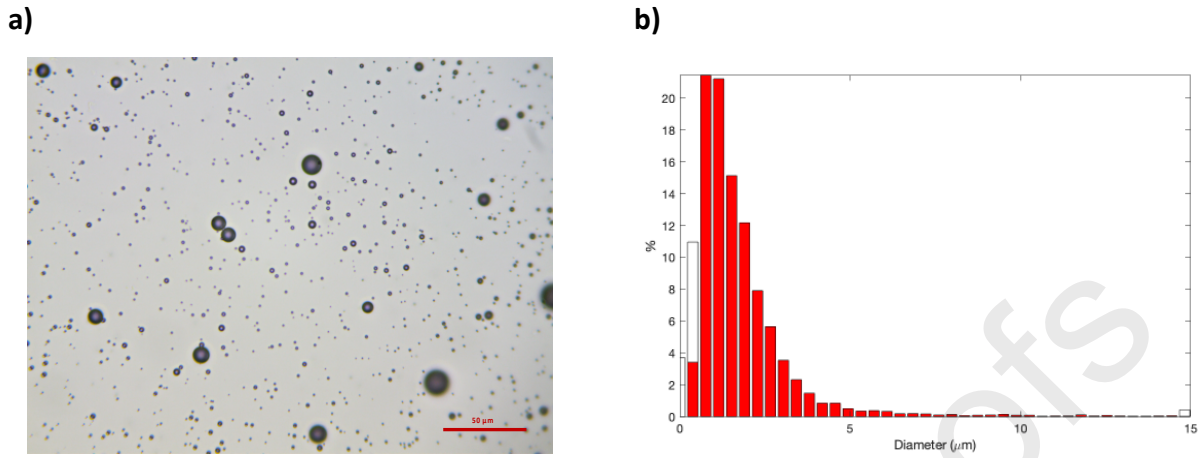

Figure 4. Representative (a) optical micrograph (1:25 dilution, scale bar represents 50 μm) and (b) size distribution analysis for Lipid-Gem MB.

a) b)

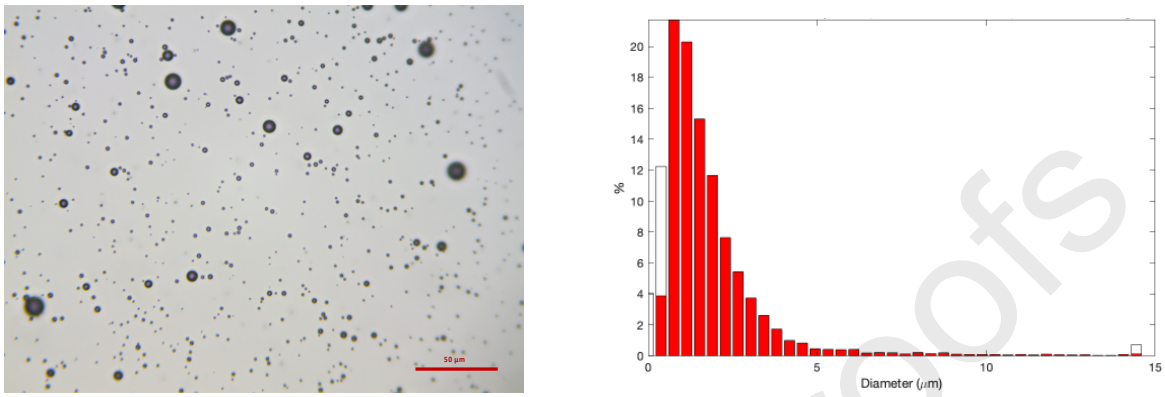

Figure 5. Representative (a) optical micrograph (1:25 dilution, scale bar represents 50 µm) and (b) size distribution analysis of Lipid-Gem-PTX MB.

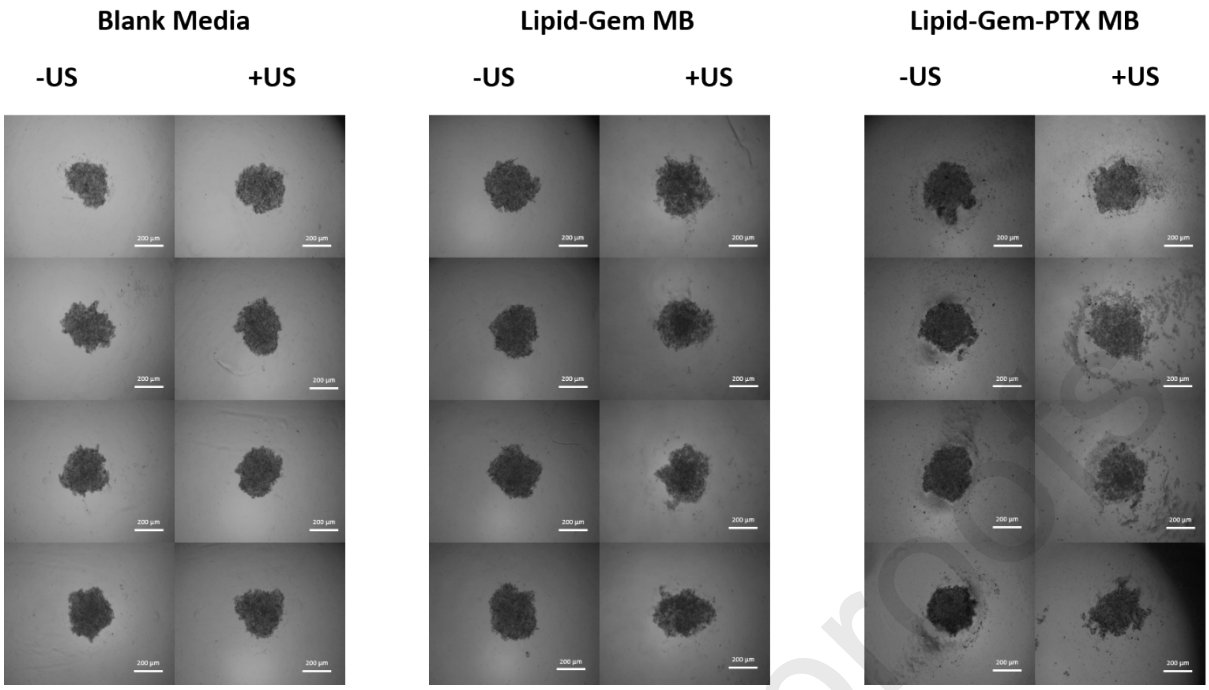

Figure 6. Representative images of PANC-1 spheroids treated with (from left to right) (i) untreated ± US (b) Lipid-Gem MB ([Lipid-Gem] = 10 μM, 3 x10^7 MB) ± US and (c) Lipid-Gem-PTX MB ([Lipid-Gem] = 10 μM, [PTX] = 6.2 μM, 3 x10^7 MB) ± US. Scale bar = 200 μm.

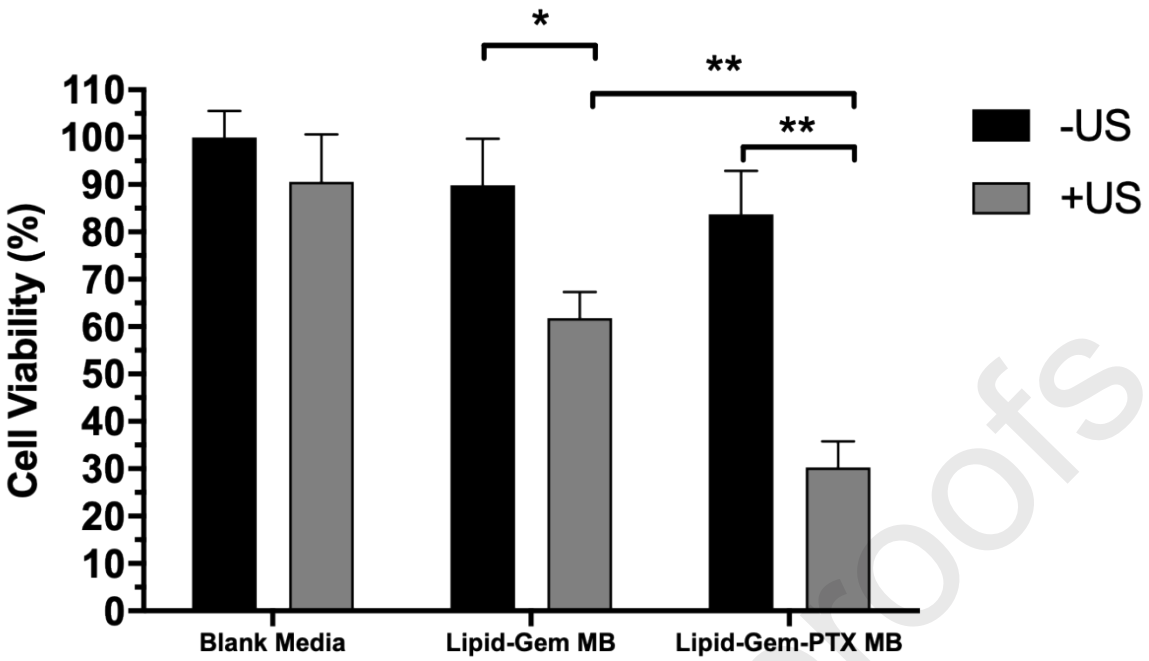

Figure 7. Plot of cell viability for the PANC-1 spheroids treated as described in Figure 6. Error bars represent ± standard error of the mean where n = 3. *p ≤ 0.05, **p ≤ 0.01.

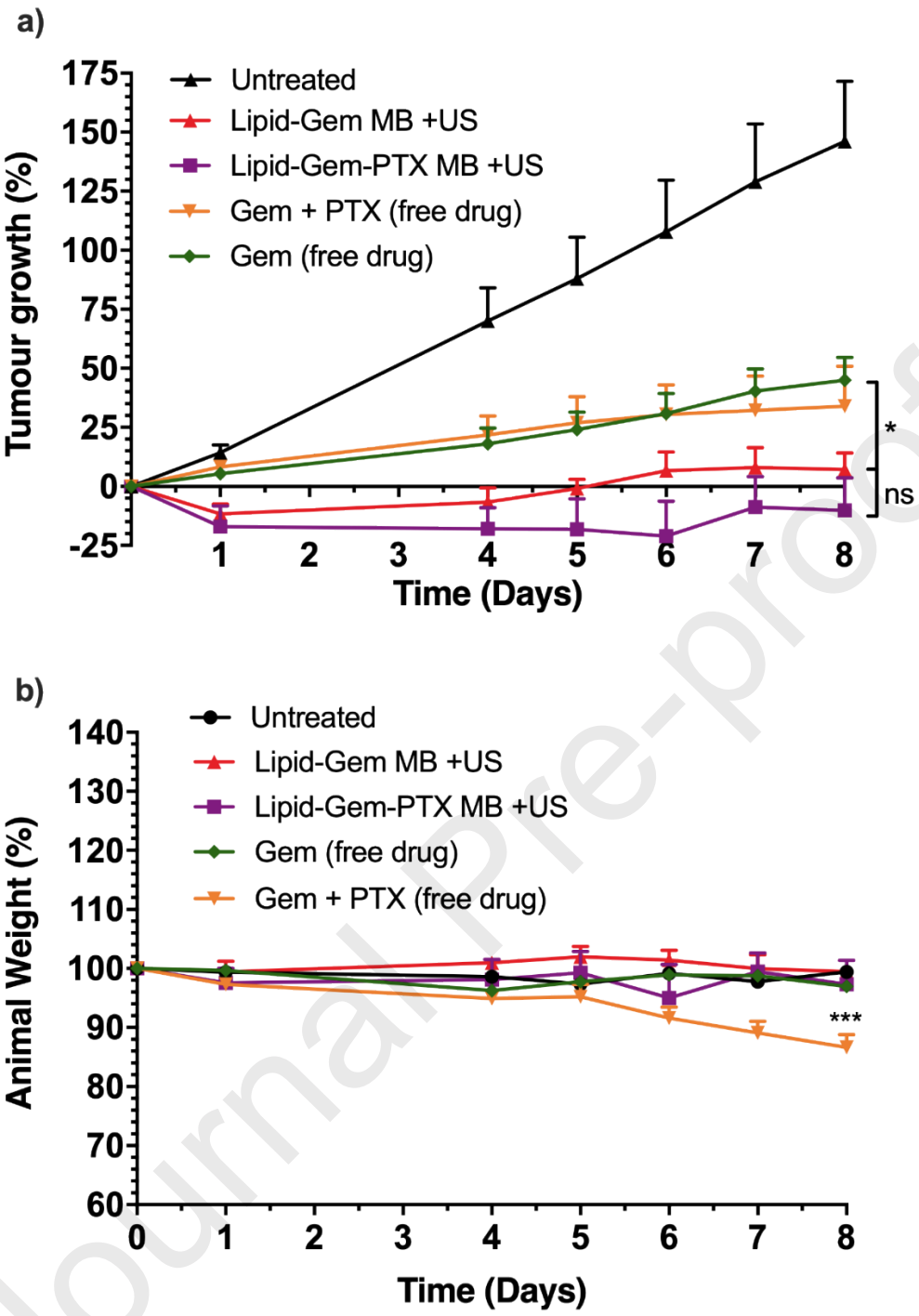

Figure 8. Plot of (a) % change in tumour volume and (b) % change in body weight for BxPC-3 tumour bearing mice that were either (i) untreated or treated with (ii) Lipid-Gem MB (iii) Lipid-Gem-PTX MB (iv) Gem (free drug) (v) Gem + PTX (free). Error bars represent ± standard error of the mean where n ≥ 4. For plot (a) *p < 0.05 for Lipid-Gem MB vs Gem (free drug) and (b) ***p < 0.001 for Gem + PTX (free drug) vs untreated.